BUILDING RESEARCH JOURNAL

VOLUME 51, 2003 NUMBER 3

CONSTANT STRAIN TRIANGULAR ELEMENT WITH EMBEDDED DISCONTINUITY BASED ON PARTITION OF UNITY

M. AUDY[1], J. KRČEK[1], M. ŠEJNOHA[1]*, J. ZEMAN[1]

The present paper illustrates formulation and implementation of a simple constant strain triangle with embedded displacement discontinuity intended for the modeling of localized damage. To arrive at such an element the partition of unity property of finite element shape functions is used to introduce the displacement discontinuity into the finite element basis. The similarity between standard two dimensional interface element and the one based on the present formulation is used to test the behavior of the new element both in bending and tension problems by examining interfacial tractions developed along a predefined interface with a given interfacial stiffnesses. The influence of the selected numerical integration rule is also explored.

Keywords: Partition of unity method, element with embedded discontinuity, contact element, interface tractions, elastic energy

1 Introduction

The phenomenological behavior of many engineering materials is characterized by a linear elastic response until their tensile strength is reached followed by the gradual loss of load capacity until failure. Experimentally obtained load-deformation curves exhibit a behavior known as a structural softening. The basic mechanisms driving the structural softening are associated with deformation processes taking place on microlevel having a character of distributed damage (e.g., microcracking) that eventually evolves into a large discrete failure mode such as cracks. At a certain stage of this process an inelastic deformation starts to localize in a small area while the rest of a structure tends to unload. This phenomenon is known as strain localization.

Within the finite element framework, the strain-softening (constitutive softening) can be included into the analysis through a suitable choice of material law. Such laws

[1] Czech Technical University in Prague, Faculty of Civil Engineering, Department of Structural Mechanics, Thákurova 7, 166 29 Prague 6

* Corresponding author

are generally phenomenological and contain no actual information about the microscopic behavior of the material. If no action is taken the combination of finite element continuum model and standard rate independent constitutive law enhanced by strain softening features of the material behavior suffers from inherited mesh dependence. The literature offers a number of ways of solving this problem through a suitable regularization of constitutive equations such as smeared crack approach, non-local models (Pijaudier-Cabot and Bažant 1987), or gradient regularized models (De Borst and Muhlhaus 1992). The common point of departure of all of these methods is the assumption of smooth continuous displacement field throughout a body. From the mechanical point of view, however, the localized failure manifests itself by macroscopical discontinuities that can be characterized as jumps in the displacement field. Thus introducing a discontinuity into a kinematic field is a natural way of modeling localized damage. This approach, which takes the name strong discontinuity, has received a considerable attention in the literature particularly in the last decade ((Moes et al. 1999; Oliver et al. 1999; Oliver et al. 2002; De Proft et al. 2002; Simone et al. 2001; Wells and Sluys et al. 2001), to cite a few).

The aim of this paper is to contribute to this field by introducing the most simple constant strain triangular element with embedded discontinuity. Apart from standard formulation of governing equations displayed in most of the referenced works this contribution also attempts to provide, in an appealing way, a clear guidance for the numerical implementation of the present element. To identify the basic features of this element including the essential ingredients of its implementation we continue in the footsteps of (Simone et al. 2001) and draw on the formal similarity with the conventional interface element to test the behavior of the new element, at present, in the limit of elastic range.

This paper is organized as follows. The strong discontinuity approach for the derivation of weak governing equations for a body crossed by a discontinuity is pursued in Section 2 to arrive at the constant strain 2-dimensional triangular element with embedded displacement discontinuities using the Partition of Unity Method (PUM). The theoretical part is completed in Section 3 that provides brief summary of the derivation of 2-dimensional interface element. Several numerical results are presented in Section 4. The comparison between PUM-like interface element and the conventional interface element outlined in Section 3 is given including the effect of high interface stiffnesses on traction oscillations. The contribution concludes by describing the discontinuity front tracking method, see Section 5.

2 Constant strain triangular element with embedded discontinuity

The present section provides derivation of a simple constant strain triangle enhanced by discontinuous shape functions to allow for jumps in the displacement field (strong discontinuity approach). In doing so the partition of unity property of the finite element shape functions is exploited. Throughout this section, the standard engineering notation is used (see, e.g., (Bittnar and Šejnoha 1996)); the stress and strain tensors written in

the vector form are given by

$$\boldsymbol{\sigma} = \{\, \sigma_{xx} \quad \sigma_{yy} \quad \sigma_{zz} \quad \sigma_{yz} \quad \sigma_{zx} \quad \sigma_{xy} \,\}^{\mathrm{T}}, \tag{1}$$

and

$$\boldsymbol{\epsilon} = \{\, \varepsilon_{xx} \quad \varepsilon_{yy} \quad \varepsilon_{zz} \quad 2\varepsilon_{yz} \quad 2\varepsilon_{zx} \quad 2\varepsilon_{xy} \,\}^{\mathrm{T}}. \tag{2}$$

We further introduce the (3×6) matrix $\boldsymbol{\partial}$ defined as

$$\boldsymbol{\partial} = \begin{bmatrix} \frac{\partial}{\partial x} & 0 & 0 & 0 & \frac{\partial}{\partial z} & \frac{\partial}{\partial y} \\ 0 & \frac{\partial}{\partial y} & 0 & \frac{\partial}{\partial z} & 0 & \frac{\partial}{\partial x} \\ 0 & 0 & \frac{\partial}{\partial z} & \frac{\partial}{\partial y} & \frac{\partial}{\partial x} & 0 \end{bmatrix}, \tag{3}$$

and the (3×6) matrix $\boldsymbol{n}$ that stores the components of unit normal vector,

$$\boldsymbol{n} = \begin{bmatrix} n_x & 0 & 0 & 0 & n_z & n_y \\ 0 & n_y & 0 & n_z & 0 & n_x \\ 0 & 0 & n_z & n_y & n_x & 0 \end{bmatrix}. \tag{4}$$

2.1 Kinematics of a displacement jump

Consider a body Ω bounded by a surface Γ and crossed by a discontinuity Γ_d, Fig 1. Γ_u represents a portion of Γ with prescribed displacements $\overline{\boldsymbol{u}}$ while tractions $\overline{\boldsymbol{t}}$ are prescribed on Γ_t ($\Gamma_u \cap \Gamma_t \cap \Gamma_d = \emptyset$). The internal discontinuity surface Γ_d divides the body into two sub-domains, Ω^+ and Ω^- ($\Omega = \Omega^+ \cup \Omega^-$). Suppose that the displacement field can be split into a discontinuous and continuous parts

$$\boldsymbol{u}(\boldsymbol{x}, t) = \widehat{\boldsymbol{u}}(\boldsymbol{x}, t) + H_{\Gamma_d}(\boldsymbol{x})\widetilde{\boldsymbol{u}}(\boldsymbol{x}, t), \tag{5}$$

where $H_{\Gamma_d}(\boldsymbol{x})$ is the Heaviside function centered at the discontinuity surface Γ_d ($H_{\Gamma_d}(\boldsymbol{x}) = 1, \forall \boldsymbol{x} \in \Omega^+$ and $H_{\Gamma_d}(\boldsymbol{x}) = 0, \forall \boldsymbol{x} \in \Omega^-$) and $\widehat{\boldsymbol{u}}$ and $\widetilde{\boldsymbol{u}}$ are continuous functions on Ω. Note that the discontinuity is introduced by the Heaviside function $H_{\Gamma_d}(\boldsymbol{x})$ at the discontinuity surface Γ_d and that the magnitude of the displacement jump $[\![\boldsymbol{u}]\!]$ at the discontinuity surface is given by $\widetilde{\boldsymbol{u}}$. For small displacements, the strain field assumes the form

$$\epsilon = \partial^{\mathrm{T}} \boldsymbol{u} = \begin{cases} \boldsymbol{\partial}^{\mathrm{T}} \widehat{\boldsymbol{u}} & \forall \boldsymbol{x} \in \Omega^-, \\ \boldsymbol{\partial}^{\mathrm{T}} \widehat{\boldsymbol{u}} + \partial^{\mathrm{T}} \widetilde{\boldsymbol{u}} & \forall \boldsymbol{x} \in \Omega^+ . \end{cases} \tag{6}$$

Comparing Eq. (5) with Eq. (6) we finally get

$$\boldsymbol{\epsilon} = \boldsymbol{\partial}^{\mathrm{T}} \widehat{\boldsymbol{u}} + H_{\Gamma_d} \boldsymbol{\partial}^{\mathrm{T}} \widetilde{\boldsymbol{u}} \quad \forall \boldsymbol{x} \in \Omega \setminus \Gamma_d. \tag{7}$$

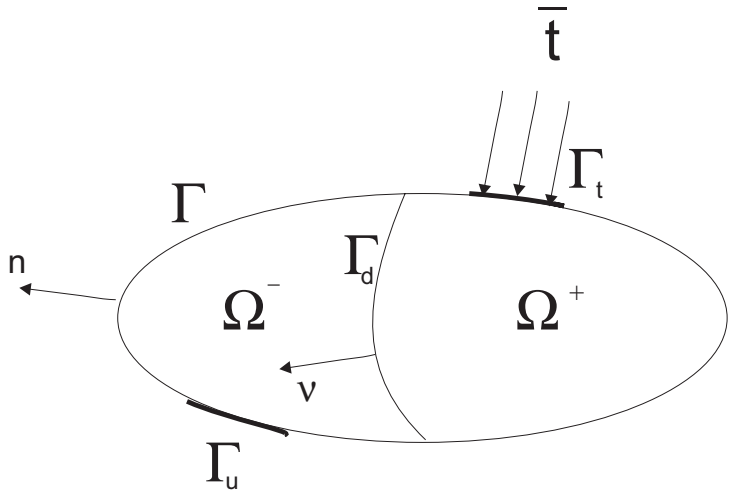

Fig. 1. Body Ω crossed by discontinuity Γ_d

2.2 Kinematics discretization

The displacement field can be interpolated over the body Ω using the concept of partition of unity method. For the purpose of this work, it is sufficient to define a partition of unity as a collection of functions φ_i which satisfy (see, e.g, (Babuška and Melenk 1997; Duarte and Oden 1996; Melenk and Babuška et al. 1996) for more details)

$$\sum_{i=1}^{n} \varphi_i(\boldsymbol{x}) = 1 \quad \forall \boldsymbol{x} \in \Omega, \tag{8}$$

where n is the number of discrete points (nodes). The displacement field will be interpolated in terms of discrete nodal values by

$$u(\boldsymbol{x}) = \sum_{i=1}^{n} \varphi_i(\boldsymbol{x}) \Big(a_i + \gamma_i(\boldsymbol{x}) b_i \Big), \tag{9}$$

where φ_i is a partition of unity function, a_i is the discrete nodal value and b_i is the 'enhanced' nodal value with respect to 'enhanced' basis γ_i. Note that the standard finite element shape functions also form a partitions of unity since

$$\sum_{i=1}^{n} N_i(\boldsymbol{x}) = 1 \quad \forall \boldsymbol{x} \in \Omega. \tag{10}$$

In the standard finite element method, the partition of unity functions are shape functions and the enhanced basis is empty. When adopting the general scheme (9), the discretized form of the displacement field becomes (Babuška and Melenk 1997; Duarte and Oden 1996; Melenk and Babuška et al. 1996)

$$\boldsymbol{u}(\boldsymbol{x}) = \mathbf{N}(\boldsymbol{x})\boldsymbol{a} + \mathbf{N}(\boldsymbol{x})(\mathbf{N}_\gamma(\boldsymbol{x})\boldsymbol{b}), \tag{11}$$

where $\mathbf{N}$ is a matrix of standard nodal shape functions to interpolate regular nodal degrees of freedom and vector $\mathbf{N}(\mathbf{N}_\gamma\boldsymbol{b})$ serves to introduce certain specific features of the displacement field $\boldsymbol{u}$ using the so called enhanced degrees of freedom stored in vector $\boldsymbol{b}$. Introduction Eq. (9) into Eq. (16), the strain field is then expressed as

$$\boldsymbol{\epsilon}(\boldsymbol{x}) = \mathbf{B}(\boldsymbol{x})\boldsymbol{a} + \mathbf{B}_\gamma(\boldsymbol{x})\boldsymbol{b}, \tag{12}$$

where $\mathbf{B} = \boldsymbol{\partial}^{\mathrm{T}}\mathbf{N}$ and $\mathbf{B}_\gamma = \boldsymbol{\partial}^{\mathrm{T}}(\mathbf{N}\mathbf{N}_\gamma)$.

A suitable choice of $\mathbf{N}_\gamma$ may considerably improve the description of the displacement field for a specific class of problems (Babuška et al. 2001). When solving, e.g., the localized damage problem, the discontinuous displacement field can be easily modeled after replacing the matrix $\mathbf{N}_\gamma$ by a scalar Heaviside function H_{Γ_d} multiplied by matrix $\mathbf{H}$ (a matrix with entry 1 if the corresponding degree of freedom is enhanced and zero otherwise). Eqs. (11) and (12) then become

$$\boldsymbol{u}(\boldsymbol{x}) = \mathbf{N}(\boldsymbol{x})\boldsymbol{a} + H_{\Gamma_d}(\boldsymbol{x})\mathbf{N}(\boldsymbol{x})\mathbf{H}\boldsymbol{b}, \tag{13}$$

$$\boldsymbol{\epsilon}(\boldsymbol{x}) = \mathbf{B}(\boldsymbol{x})\boldsymbol{a} + H_{\Gamma_d}(\boldsymbol{x})\mathbf{B}(\boldsymbol{x})\mathbf{H}\boldsymbol{b}, \tag{14}$$

where Eq. (14) holds for $\boldsymbol{x} \in \Omega \setminus \Gamma_d$.

2.3 Governing equations

Consider a linear elastic body Ω. Assuming small strains and zero body forces, the linear momentum balance equation and the kinematic equations result in

$$\boldsymbol{\partial}\boldsymbol{\sigma} = \mathbf{0}, \tag{15}$$

and

$$\boldsymbol{\epsilon} = \boldsymbol{\partial}^{\mathrm{T}}\boldsymbol{u}. \tag{16}$$

The traction and displacement boundary conditions are given by

$$\boldsymbol{n}\boldsymbol{\sigma} = \overline{\boldsymbol{t}} \quad \text{on } \Gamma_t, \tag{17}$$

and

$$\boldsymbol{u} = \overline{\boldsymbol{u}} \quad \text{on} \Gamma_u. \tag{18}$$

The system of governing equations is usually derived by invoking the principle of virtual work. In particular, the principle of virtual displacements can be recovered by forcing the equations of equilibrium, Eq. (15), to be satisfied in average sense such that

$$\int_\Omega \delta \boldsymbol{u}^{\mathrm{T}} (\boldsymbol{\partial} \boldsymbol{\sigma}) \, \mathrm{d}\Omega = 0, \tag{19}$$

for all statically admissible $\delta \boldsymbol{u}$. Splitting the above integral into continuous and discontinuous parts we get

$$\int_\Omega \delta \widehat{\boldsymbol{u}}^{\mathrm{T}} (\boldsymbol{\partial} \boldsymbol{\sigma}) \, \mathrm{d}\Omega + \int_\Omega H_{\Gamma_d} \delta \widetilde{\boldsymbol{u}}^{\mathrm{T}} (\boldsymbol{\partial} \boldsymbol{\sigma}) \, \mathrm{d}\Omega = 0, \tag{20}$$

for all statically admissible $\delta \widehat{\boldsymbol{u}}$ and $\delta \widetilde{\boldsymbol{u}}$. Taking into account the fact that $H_{\Gamma_d} = 0$ on Ω^- we write individual integrals with the help of Green's theorem, formula for distributional derivative of the Heaviside function and Eq. (17) as

$$\int_\Omega \delta \widehat{\boldsymbol{u}}^{\mathrm{T}} (\boldsymbol{\partial} \boldsymbol{\sigma}) \, \mathrm{d}\Omega = \int_{\Gamma_t} \delta \widehat{\boldsymbol{u}}^{\mathrm{T}} \overline{\boldsymbol{t}} \, \mathrm{d}\Gamma - \int_\Omega \left(\boldsymbol{\partial}^{\mathrm{T}} \delta \widehat{\boldsymbol{u}} \right)^{\mathrm{T}} \boldsymbol{\sigma} \, \mathrm{d}\Omega, \tag{21}$$

$$\begin{aligned} \int_\Omega H_{\Gamma_d} \delta \widetilde{\boldsymbol{u}}^{\mathrm{T}} (\boldsymbol{\partial} \boldsymbol{\sigma}) \, \mathrm{d}\Omega &= \int_{\Gamma_t} H_{\Gamma_d} \delta \widetilde{\boldsymbol{u}}^{\mathrm{T}} \overline{\boldsymbol{t}} \, \mathrm{d}\Gamma - \int_\Omega \left(\boldsymbol{\partial}^{\mathrm{T}} \left(H_{\Gamma_d} \delta \widetilde{\boldsymbol{u}} \right) \right)^{\mathrm{T}} \boldsymbol{\sigma} \, \mathrm{d}\Omega \\ &= \int_{\Gamma_t^+} \delta \widetilde{\boldsymbol{u}}^{\mathrm{T}} \overline{\boldsymbol{t}} \, \mathrm{d}\Gamma - \int_{\Gamma_d} \delta \widetilde{\boldsymbol{u}}^{\mathrm{T}} \boldsymbol{t} \, \mathrm{d}\Gamma - \int_{\Omega^+} \left(\boldsymbol{\partial}^{\mathrm{T}} \delta \widetilde{\boldsymbol{u}} \right)^{\mathrm{T}} \boldsymbol{\sigma} \, \mathrm{d}\Omega. \end{aligned} \tag{22}$$

Comparing Eqs. (21) and (22) with Eq. (19) and taking into account the independence of variations $\delta \widehat{\boldsymbol{u}}$ and $\delta \widetilde{\boldsymbol{u}}$ we arrive at the weak form of governing equations

$$\int_\Omega \left(\boldsymbol{\partial}^{\mathrm{T}} \delta \widehat{\boldsymbol{u}} \right)^{\mathrm{T}} \boldsymbol{\sigma} \, \mathrm{d}\Omega = \int_{\Gamma_t} \delta \widehat{\boldsymbol{u}}^{\mathrm{T}} \overline{\boldsymbol{t}} \, \mathrm{d}\Gamma, \tag{23}$$

$$\int_{\Omega^+} \left(\boldsymbol{\partial}^{\mathrm{T}} \delta \widetilde{\boldsymbol{u}} \right)^{\mathrm{T}} \boldsymbol{\sigma} \, \mathrm{d}\Omega + \int_{\Gamma_d} \delta \widetilde{\boldsymbol{u}}^{\mathrm{T}} \boldsymbol{t} \, \mathrm{d}\Gamma = \int_{\Gamma_t^+} \delta \widetilde{\boldsymbol{u}}^{\mathrm{T}} \overline{\boldsymbol{t}} \, \mathrm{d}\Gamma. \tag{24}$$

Finally, inserting the discrete form of Eqs. (13)–(14) into Eqs. (23)–(24) and employing constitutive equations for the stress $\boldsymbol{\sigma}$ at a point $\boldsymbol{x} \in \Omega \setminus \Gamma_d$

$$\boldsymbol{\sigma} = \widehat{\mathbf{D}} \boldsymbol{\epsilon} = \widehat{\mathbf{D}} \left(\mathbf{B} \boldsymbol{a} + H_{\Gamma_d} \mathbf{B} \boldsymbol{b} \right), \tag{25}$$

and tractions developed on the discontinuity surface Γ_d

$$\boldsymbol{t} = \widetilde{\mathbf{D}} \mathbf{N} \boldsymbol{b}, \tag{26}$$

yields

$$\int_{\Omega} \mathbf{B}^{\mathrm{T}} \widehat{\mathbf{D}} \mathbf{B} \boldsymbol{a} \, \mathrm{d}\Omega + \int_{\Omega^+} \mathbf{B}^{\mathrm{T}} \widehat{\mathbf{D}} \mathbf{B} \boldsymbol{b} \, \mathrm{d}\Omega = \int_{\Gamma_t} \mathbf{N}^{\mathrm{T}} \overline{\boldsymbol{t}} \, \mathrm{d}\Gamma, \tag{27}$$

$$\int_{\Omega^+} \mathbf{B}^{\mathrm{T}} \widehat{\mathbf{D}} \mathbf{B} \boldsymbol{a} \, \mathrm{d}\Omega + \int_{\Omega^+} \mathbf{B}^{\mathrm{T}} \widehat{\mathbf{D}} \mathbf{B} \boldsymbol{b} \, \mathrm{d}\Omega + \int_{\Gamma_d} \mathbf{N}^{\mathrm{T}} \widetilde{\mathbf{D}} \mathbf{N} \boldsymbol{b} \, \mathrm{d}\Gamma = \int_{\Gamma_t^+} \mathbf{N}^{\mathrm{T}} \overline{\boldsymbol{t}} \, \mathrm{d}\Gamma. \tag{28}$$

The resulting discrete system of linear equations has the traditional form

$$\mathbf{K} \boldsymbol{u} = \boldsymbol{f}, \tag{29}$$

where $\boldsymbol{u}$ represents the vector of nodal displacements consisting of standard and enhanced degrees of freedom

$$\boldsymbol{u} = \{ \, \boldsymbol{a} \quad \boldsymbol{b} \, \}^{\mathrm{T}}, \tag{30}$$

and $\boldsymbol{f}$ lists externally applied forces

$$\boldsymbol{f} = \{ \, \boldsymbol{f}_a \quad \boldsymbol{f}_b \, \}^{\mathrm{T}}, \tag{31}$$

where

$$\boldsymbol{f}_a = \int_{\Gamma_t} \mathbf{N}^{\mathrm{T}} \overline{\boldsymbol{t}} \, \mathrm{d}\Gamma, \tag{32}$$

$$\boldsymbol{f}_b = \int_{\Gamma_t^+} \mathbf{N}^{\mathrm{T}} \overline{\boldsymbol{t}} \, \mathrm{d}\Gamma, \tag{33}$$

and finally $\mathbf{K}$ represents the enhanced stiffness matrix

$$\mathbf{K} = \begin{bmatrix} \mathbf{K}_{aa} & \mathbf{K}_{ab} \\ \mathbf{K}_{ba} & \mathbf{K}_{bb} \end{bmatrix}, \tag{34}$$

where individual sub-matrices are defined as

$$\mathbf{K}_{aa} = \int_{\Omega} \mathbf{B}^{\mathrm{T}} \widehat{\mathbf{D}} \mathbf{B} \, \mathrm{d}\Omega, \tag{35}$$

$$\mathbf{K}_{ab} = \mathbf{K}_{ba}{}^{\mathrm{T}} = \int_{\Omega^+} \mathbf{B}^{\mathrm{T}} \widehat{\mathbf{D}} \mathbf{B} \, \mathrm{d}\Omega, \tag{36}$$

$$\mathbf{K}_{bb} = \int_{\Omega^+} \mathbf{B}^{\mathrm{T}} \widehat{\mathbf{D}} \mathbf{B} \, \mathrm{d}\Omega + \int_{\Gamma_d} \mathbf{N}^{\mathrm{T}} \widetilde{\mathbf{D}} \mathbf{N} \, \mathrm{d}\Gamma. \tag{37}$$

Following the standard finite element procedure, the enhanced stiffness matrix is obtained by the assembly of contribution from individual elements. To that end, the domain Ω is decomposed into N_e non-intersecting elements Ω_e such that $\Omega = \cup_{e=1}^{N_e} \Omega_e$. Formally writing, the global stiffness matrix and the global force vector become

$$\mathbf{K} = \mathsf{A}_{e=1}^{N_e} \mathbf{K}_e, \tag{38}$$

$$\boldsymbol{f} = \mathsf{A}_{e=1}^{N_e} \boldsymbol{f}_e, \tag{39}$$

where non-zero contributions to enhanced degrees of freedom come either from the elements crossed by the discontinuity,

$$\mathbf{K}_{aa,e} = \int_{\Omega_e} \mathbf{B}_e{}^{\mathrm{T}} \widehat{\mathbf{D}}_e \mathbf{B}_e \, \mathrm{d}\Omega, \tag{40}$$

$$\mathbf{K}_{ab,e} = \mathbf{K}_{ba,e}{}^{\mathrm{T}} = \int_{\Omega_e^+} \mathbf{B}_e{}^{\mathrm{T}} \widehat{\mathbf{D}}_e \mathbf{B}_e \, \mathrm{d}\Omega, \tag{41}$$

$$\mathbf{K}_{bb,e} = \int_{\Omega_e^+} \mathbf{B}_e{}^{\mathrm{T}} \widehat{\mathbf{D}}_e \mathbf{B}_e \, \mathrm{d}\Omega + \int_{\Gamma_{d,e}} \mathbf{N}_e{}^{\mathrm{T}} \widetilde{\mathbf{D}}_\mathbf{e} \mathbf{N}_e \, \mathrm{d}\Gamma \tag{42}$$

or from elements, which are not crossed by a discontinuity but are contained in both the support of nodal basis function related to an enhanced degree of freedom and the Heaviside function. Then, ${\Omega_e}^+ = \Omega_e$ and the contribution from the discontinuity (the second term on the right hand side of Eq. (42)) is zero.

2.4 Triangular element

For the 2-dimensional analysis the most simple isoparametric constant strain triangular element with linear shape functions, extended by including the enhanced degrees of freedom to enable discontinuity modeling, is derived. The main advantage of a triangular family of elements is the possibility of their adapting to virtually any shape and relative easiness of their implementation. The element is represented by four degrees of freedom in each node. In particular, two standard and two enhanced degrees of freedom serve to describe fully the displacement field within an element. Unlike the original formulation, where the displacements were ordered by degrees of freedom, the ordering of unknowns is now as follows

$$\boldsymbol{u} = \{\, \widehat{u}_1 \quad \widehat{v}_1 \quad \widetilde{u}_1 \quad \widetilde{v}_1 \quad \widehat{u}_2 \quad \widehat{v}_2 \quad \widetilde{u}_2 \quad \widetilde{v}_2 \quad \widehat{u}_3 \quad \widehat{v}_3 \quad \widetilde{u}_3 \quad \widetilde{v}_3 \,\}^{\mathrm{T}}, \tag{43}$$

where $\widehat{\boldsymbol{u}}$ and $\widehat{\boldsymbol{v}}$ represent standard displacement degrees of freedom in the x and y coordinate system, respectively. The corresponding enhanced degrees of freedom are $\widetilde{\boldsymbol{u}}$ and $\widetilde{\boldsymbol{v}}$. This ordering displayed in Fig. 2 together with the assumed integration points then allows the use of standard FEM solver. The shape functions for an isoparametric

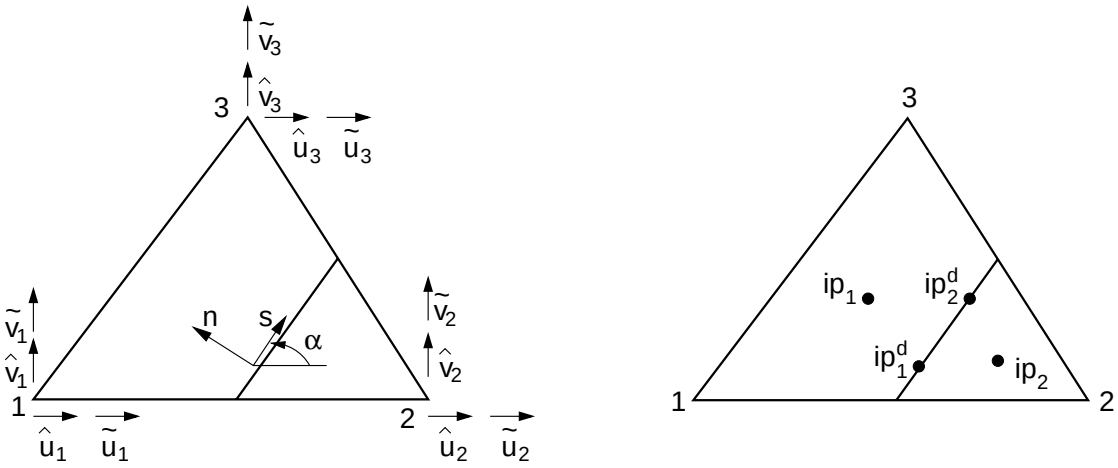

Fig. 2. Standard and enhanced degrees of freedom for a triangular element and selected Gauss integration points within the element and on the discontinuity

enhanced triangular element can be defined in terms of area functions as (Bittnar and Šejnoha 1996)

$$\mathbf{N} = [\, L_1 \quad L_1 \quad L_1 \quad L_1 \quad L_2 \quad L_2 \quad L_2 \quad L_2 \quad L_3 \quad L_3 \quad L_3 \quad L_3 \,], \tag{44}$$

where L_i is the function of position (x, y) and element node coordinates x_i, y_i, $i = 1, 2, 3$

$$L_1 = \frac{a_1 + b_1 x + c_1 y}{2A}$$
$$L_2 = \frac{a_2 + b_2 x + c_2 y}{2A}$$
$$L_3 = \frac{a_3 + b_3 x + c_3 y}{2A},$$

where

$$A = \frac{1}{2} \begin{vmatrix} 1 & x_1 & y_1 \\ 1 & x_2 & y_2 \\ 1 & x_3 & y_3 \end{vmatrix} \tag{45}$$

$$a_i = x_i y_k - x_j y_i \tag{46}$$
$$b_i = y_j - y_k$$
$$c_i = x_k - x_j. \tag{47}$$

The enhanced matrix $\mathbf{B}$ can be written as

$$\mathbf{B}(\boldsymbol{x}) = \frac{1}{2A}\begin{bmatrix} b_1 & 0 & b_2 & 0 & b_3 & 0 & H(\boldsymbol{x})b_1 & 0 & H(\boldsymbol{x})b_2 & 0 & H(\boldsymbol{x})b_3 & 0 \\ 0 & c_1 & 0 & c_2 & 0 & c_3 & 0 & H(\boldsymbol{x})c_1 & 0 & H(\boldsymbol{x})c_2 & 0 & H(\boldsymbol{x})c_3 \\ c_1 & b_1 & c_2 & b_2 & c_3 & b_3 & H(\boldsymbol{x})c_1 & H(\boldsymbol{x})b_1 & H(\boldsymbol{x})c_2 & H(\boldsymbol{x})b_2 & H(\boldsymbol{x})c_3 & H(\boldsymbol{x})b_3 \end{bmatrix} \tag{48}$$

where H denotes the value of Heaviside function at a point $\boldsymbol{x}$. Assuming plane stress conditions the material stiffness matrix $\mathbf{D}$ is provided by

$$\widehat{\mathbf{D}} = \frac{E}{1-\nu^2}\begin{bmatrix} 1 & \nu & 0 \\ \nu & 1 & 0 \\ 0 & 0 & 2(1+\nu) \end{bmatrix}. \tag{49}$$

The (2×2) discontinuity material stiffness matrix $\widetilde{\mathbf{D}}_{\text{local}}$ given in the local coordinate system attains the form

$$\widetilde{\mathbf{D}}_{\text{local}} = \begin{bmatrix} K_s & 0 \\ 0 & K_n \end{bmatrix}, \tag{50}$$

where K_s and K_n are the discontinuity stiffnesses in tangential and normal directions, respectively. Using the transformation of coordinates the discontinuity material stiffness $\widetilde{\mathbf{D}}$ now written in the global coordinate system becomes

$$\widetilde{\mathbf{D}} = \mathbf{T}^{\mathrm{T}}\widetilde{\mathbf{D}}_{\text{local}}\mathbf{T}, \tag{51}$$

where $\mathbf{T}$ is the familiar transformation matrix

$$\mathbf{T} = \begin{bmatrix} \cos\alpha & \sin\alpha \\ -\sin\alpha & \cos\alpha \end{bmatrix}, \tag{52}$$

and α represents the angle between the crack alignment and the global x axis.

Using the enhanced matrix $\mathbf{B}$, the part of the element stiffness matrix containing the area integrals, see Eq. (40)–(42), can be written in a compact form as

$$\mathbf{K}_e^1 = \sum_{j=1}^{2} w_i \mathbf{B}(\boldsymbol{ip}_j)^{\mathrm{T}}\widehat{\mathbf{D}}\mathbf{B}(\boldsymbol{ip}_j), \tag{53}$$

where the integration weights w_i are given as areas of triangular and quadrilateral parts of the element (see Section 5 for more detailed discussion). The contribution corresponding to the discontinuity Γ_d is computed either by standard two-point Gaussian quadrature or by Newton-Cotes formulae, respectively,

$$\mathbf{K}_{bb,e}^2 = \sum_{j=1}^{2} \xi_j \mathbf{N}(\boldsymbol{ip^d}_j)^{\mathrm{T}}\widetilde{\mathbf{D}}\mathbf{N}(\boldsymbol{ip^d}_j), \tag{54}$$

where ξ_j and $\boldsymbol{ip^d}_j$ are the integration weights and points of a selected integration scheme. Finally, the element stiffness matrix assumes the form

$$\mathbf{K}_e = \begin{bmatrix} \mathbf{K}^1_{aa,e} & \mathbf{K}^1_{ab,e} \\ \mathbf{K}^1_{ab,e}{}^{\mathrm{T}} & \mathbf{K}^1_{bb,e} + \mathbf{K}^2_{bb,e} \end{bmatrix}. \tag{55}$$

3 Interface element

As intimated in the introductory part the behavior of the element presented in Section 3 will be tested by comparing its response to the one predicted by conventional contact elements. It thus appears reasonable to provide at least a brief summary of the derivation of the four node 2-dimensional contact element that is compatible with the three noded triangular element considered in the present study.

3.1 Basic theory

The stress-displacement relationship of the interface model assumes the form

$$\begin{Bmatrix} \tau \\ \sigma \end{Bmatrix} = [\,\widetilde{\mathbf{D}}\,] \begin{Bmatrix} [\![u]\!]_l \\ [\![v]\!]_l \end{Bmatrix}, \tag{56}$$

where $[\![u]\!]_l$ and $[\![v]\!]_l$ represent the relative displacements of the top and bottom of the interface element in the local coordinate system, Fig. 3. For isotropic linear elastic behavior the interface material stiffness matrix $\widetilde{\mathbf{D}}$ takes the form

$$\widetilde{\mathbf{D}} = \begin{bmatrix} K_s & 0 \\ 0 & K_n \end{bmatrix}, \tag{57}$$

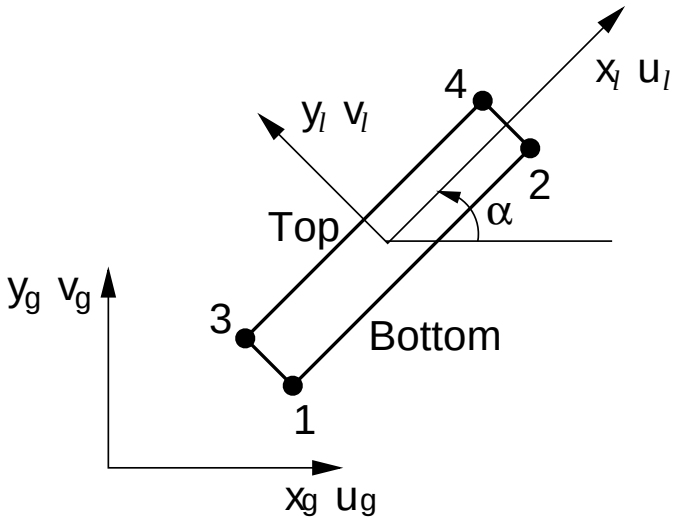

Fig. 3. Interface element

where K_s and K_n are in analogy with Eq. (50) the elastic shear and normal stiffnesses, respectively.

3.2 Finite element formulation

In the finite element framework the global displacements are approximated using the standard shape functions as

$$\begin{aligned} u^{top} &= N_1 u_3 + N_2 u_4, \\ u^{bot} &= N_1 u_1 + N_2 u_2, \\ v^{top} &= N_1 v_3 + N_2 v_4, \\ v^{bot} &= N_1 v_1 + N_2 v_2, \end{aligned} \tag{58}$$

where the global nodal degrees of freedom u_i, v_i, now written in the compact form

$$\boldsymbol{r}_g = \{u_1, v_1, u_2, v_2, u_3, v_3, u_4, v_4\}^{\mathrm{T}}, \tag{59}$$

are related to local displacement jumps

$$\left\{ \begin{array}{c} [\![u]\!]_l \\ [\![v]\!]_l \end{array} \right\} = \mathbf{B}\boldsymbol{r}_g, \tag{60}$$

where the matrix $\mathbf{B}$ assumes the form

$$\mathbf{B} = [-\mathbf{T}\mathbf{B}_1 \;\; -\mathbf{T}\mathbf{B}_2 \;\; \mathbf{T}\mathbf{B}_1 \;\; \mathbf{T}\mathbf{B}_2], \tag{61}$$

and

$$\mathbf{T} = \begin{bmatrix} \cos\alpha & \sin\alpha \\ -\sin\alpha & \cos\alpha \end{bmatrix} \qquad \mathbf{B}_i = \begin{bmatrix} N_i & 0 \\ 0 & N_i \end{bmatrix}. \tag{62}$$

The element stiffness $\mathbf{K}_e$ then follows from

$$\mathbf{K}_e = \int_{-1}^{1} \mathbf{B}^{\mathrm{T}} \widetilde{\mathbf{D}} \mathbf{B} J \, \mathrm{d}\xi, \tag{63}$$

where J is the element jacobian.

4 Example results

In this section we present several example problems that demonstrate the behavior of both the conventional interface element and element with embedded displacement discontinuity. The response of the interface element subject to bending loading is examined first. In particular, we focus on the effect of the selected integration rule on the resulting interface tractions. Similar results are presented for the discontinuous triangular element and compared to the former one.

Geometry and loading conditions of the selected problems are shown in Figs. 4 and 5. As for the material properties we assumed concrete with the Young modulus E equal to 35 MPa and the Poisson ratio ν equal to 0.3.

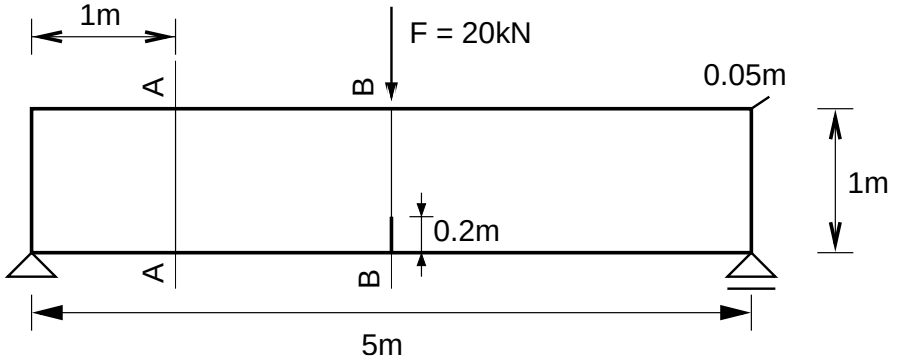

Fig. 4. 3-point bending

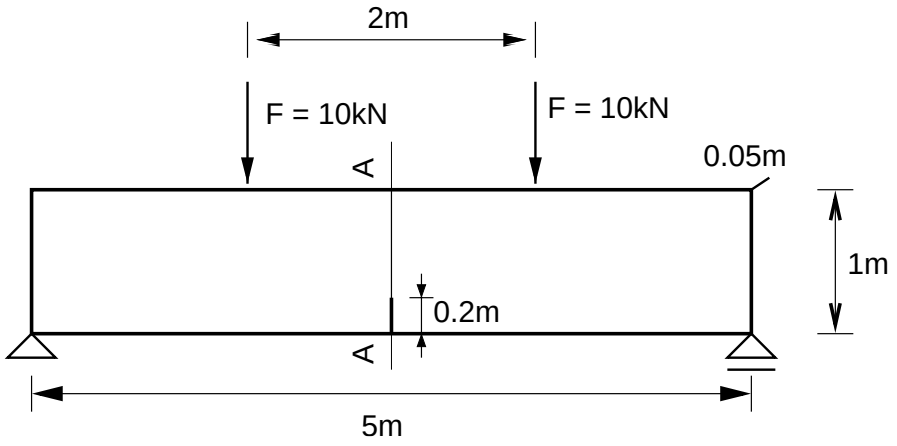

Fig. 5. 5-point bending

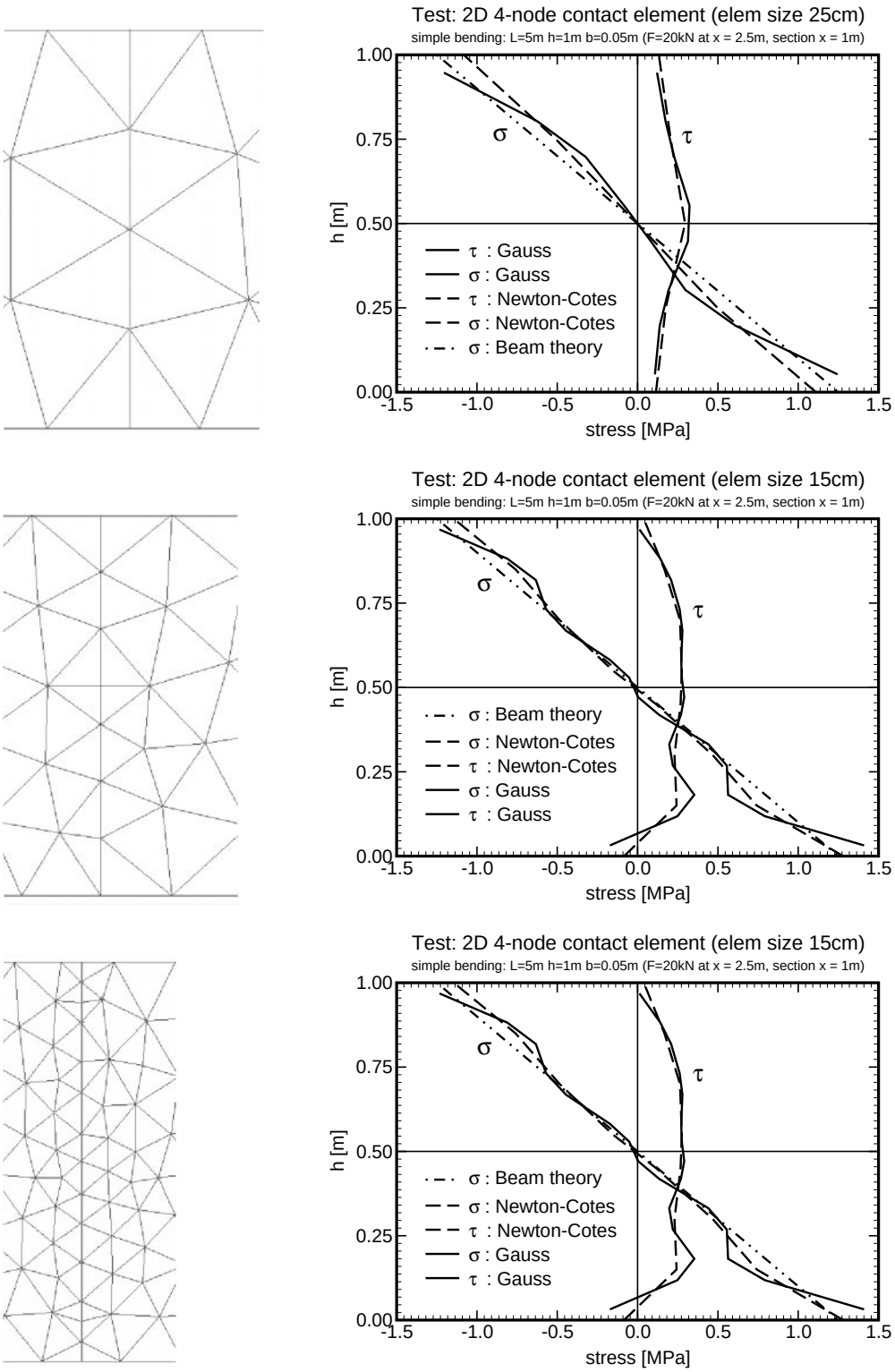

Fig. 6. 3-point bending – Distribution of normal and shear stresses in section A-A, Fig. 4

4.1 Conventional interface element

In the first example the attention was given to the distribution of normal and shear stresses in the beam section as a function of the element size. Three different meshes, Fig. 6, were considered. Corresponding results showing the distribution of normal and shear stresses over the beam height developed in section A-A are evident from Fig. 6. As expected, refining the finite element mesh considerably improves the predicted response and both integration schemes give similar results. Fig. 6 also suggests that for coarser meshes the element formulation based on the Newton-Cotes integration rule provides slightly better results. No significant oscillation of stresses as often reported with the use of interface elements is evident in this particular example even when relatively high stiffnesses $K_s = K_n = 10^6$ GN/m^3 were used. The normal stress distribution derived from the beam theory is added for comparison.

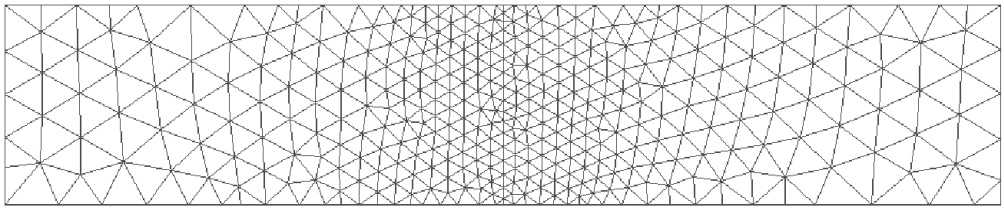

Fig. 7. 3-point bending - Finite element mesh used with interface element analysis

As the next example we studied a notch problem. Again, a three-point bending test was performed. But in this case a notch of length 20 cm was introduced in the structure, see Fig. 4. The finite element mesh used in this example appears in Fig. 7. Both the influence of interfacial stiffness and integration rule were examined. Fig. 8.1 clearly shows the difference between two integration rules, particularly when high stiffness of the interface is used. While no oscillation is detected with the Newton-Cotes integration rule, the Gauss integration scheme results in a significant oscillation of normal stresses in front of the notch tip. The similar conclusion can be drawn from Fig. 8.3. This effect, however, becomes less pronounced when reducing the interfacial stiffness. Also, one may argue that using the Noten-Cotes integration scheme hides on the other hand the true solution by smoothing out the steep gradients when larger elements are used. This effect, however, has not been examined in the present contribution. Thus in view of Figs. 8.1–8.3 the use of the Newton-Cotes integration rule at least in applications where an interface element is used to track the displacement discontinuity is preferable. Also note a relatively fine mesh used with the present problem, Fig. 7. A slight detour of the stress variation from a straight line at the top of the beam is attributed to the applied force placed in the nodes of the interface element.

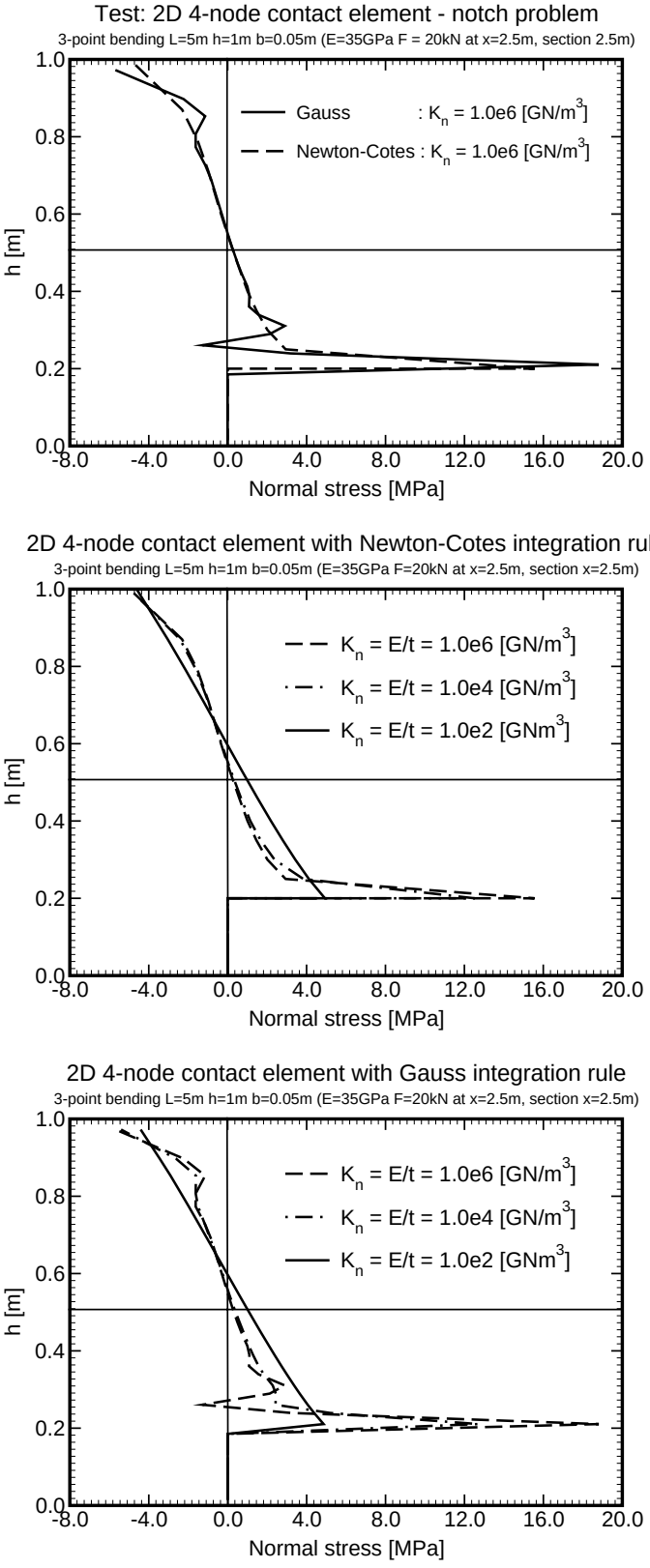

Fig. 8. 3-point bending – Distribution of normal stress in section B-B for notched specimen, Fig. 4

4.2 Constant strain triangle with embedded discontinuity

Several example problems are presented in this section to asses the behavior and applicability of the constant strain triangle enhanced by adding discontinuous shape functions. Apart from the apparent application in problems of crack propagation, the formulation of this element presented in Section 3 advocates its possible substitution for a conventional interface element, thus avoiding the need for structured meshes. To either confirm or uproot this suggestion we run a similar set of problems as in the previous section.

One of the obstacles in using this element is an application of loading along the boundary where enhanced degrees of freedom are activated. In the first set of examples this problem was eliminated by loading the beam in four-point bending, Fig. 5, so the forces were applied away from the discontinuity. Also note that closing the discontinuity on the beam edge, setting enhanced degrees of freedom associated with a given element edge to zero, solves this problem. The effects of closing the discontinuity at the top of the beam appears in Fig. 9. While in Fig. 9.1 we force the discontinuity to be closed at the top of the beam, in Fig. 9.2 the normal displacement jump at that point is free to develop, which corresponds to reality. Also note almost zero displacement jump in both cases associated with a relatively high interfacial stiffness.

The corresponding stress distributions are plotted in Fig. 10. An important conclusion can be drawn immediately when inspecting Fig. 10. The present enhanced triangular element suffers from oscillation of tractions developed along the discontinuity when modeling perfect bond through a high interfacial stiffness. This undesirable feature applies to both integration schemes. On the other hand the stress oscillations completely disappear when considerably reducing the interfacial stiffness. This situation, however, might not seem to be so critical as even with a relatively low interfacial stiffness one may arrive at reasonably accurate results. See Fig. 11 showing comparison between the interface element and the triangular one.

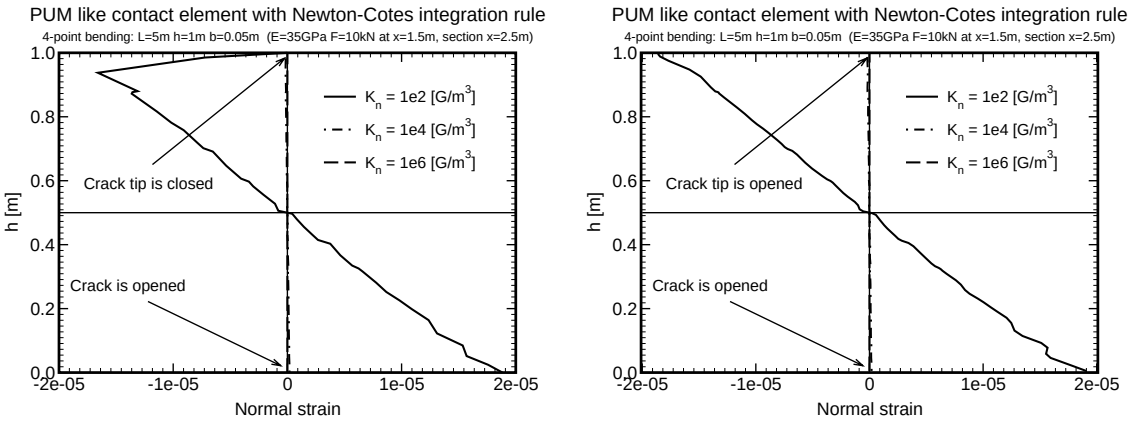

Fig. 9. 4-point bending – Distribution of normal displacement jump in sec. A-A, Fig. 5

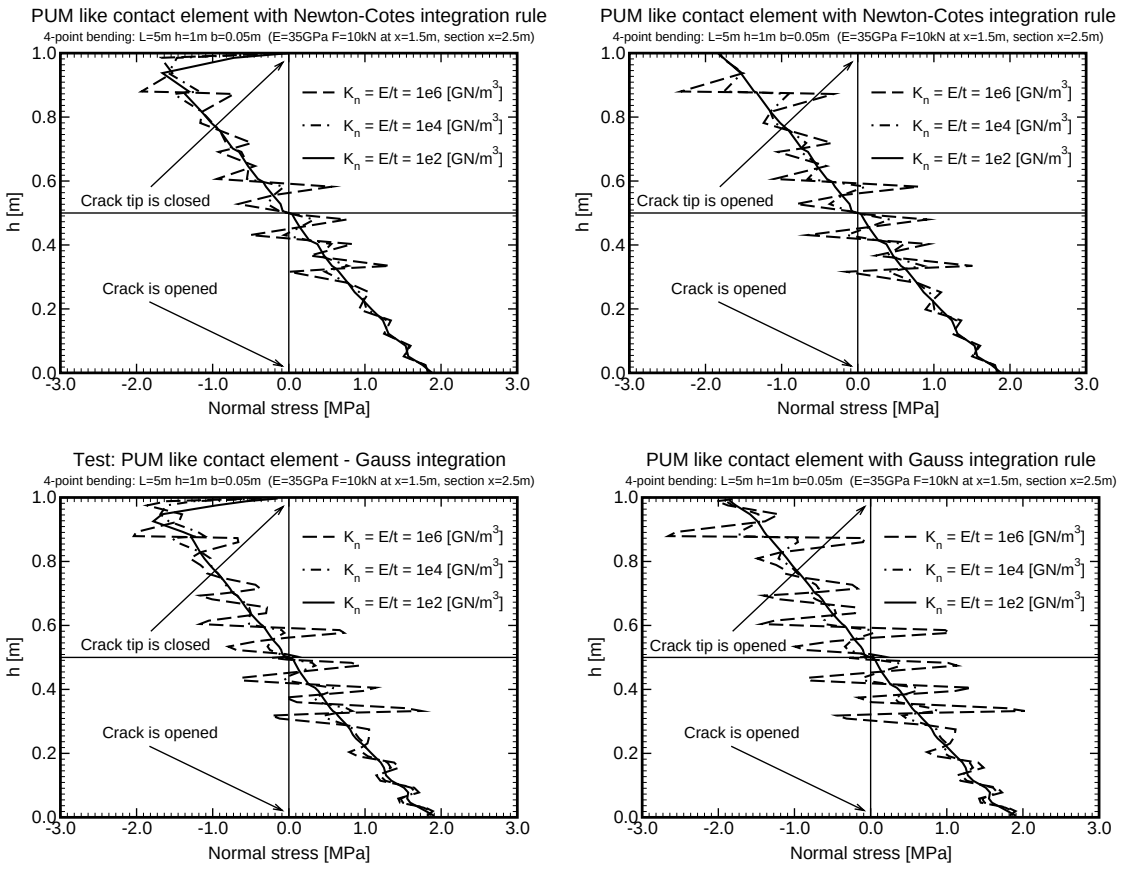

Fig. 10. 4-point bending – Distribution of normal stresses in section A-A, Fig. 5

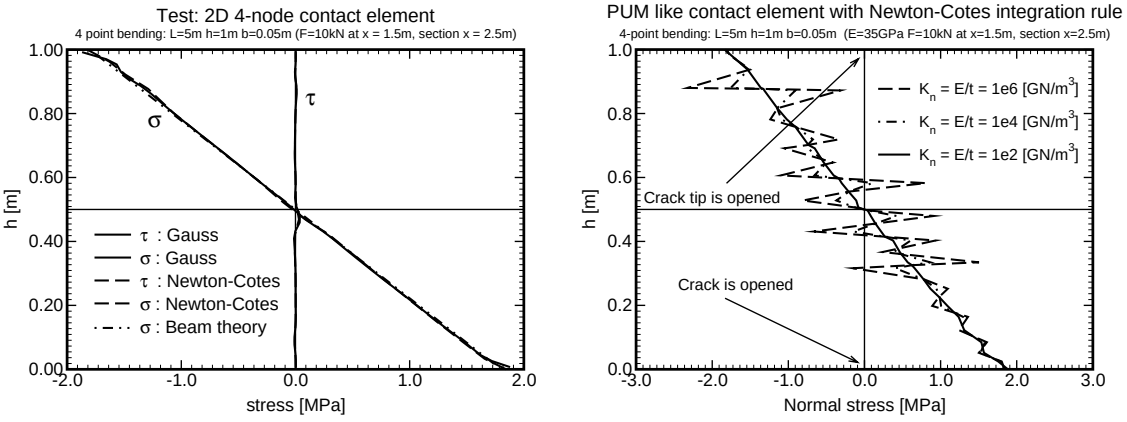

Fig. 11. 4-point bending – Distribution of normal stress in section A-A, Fig. 5

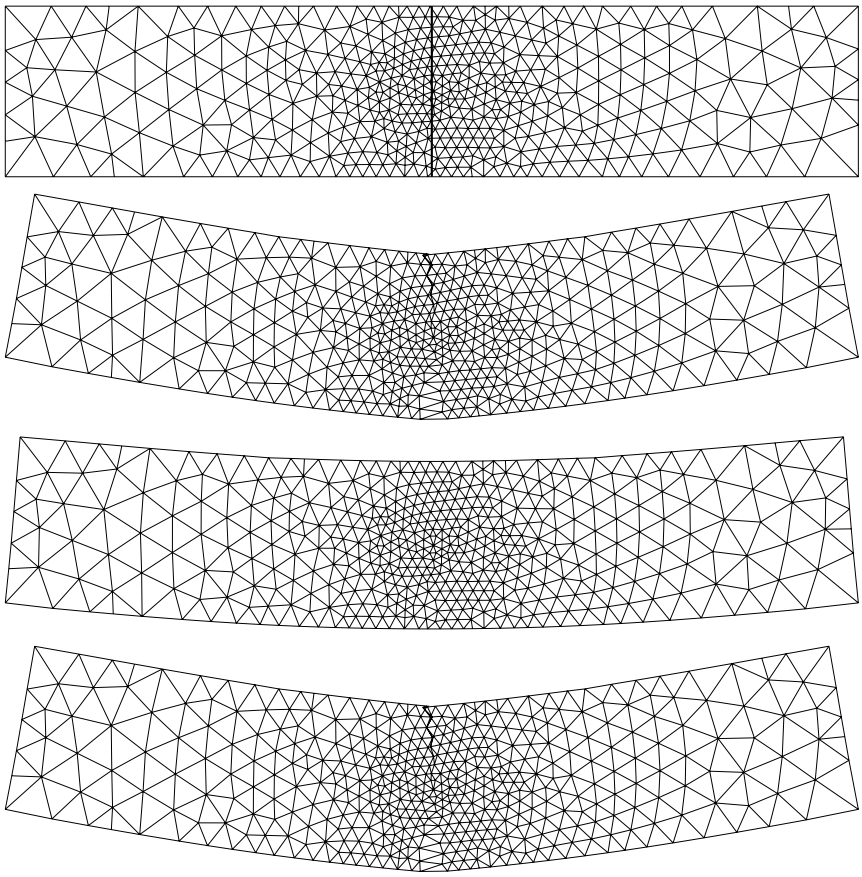

Fig. 12. 4-point bending – Finite element mesh and deformation patterns: 1. $K_n = 10^6$ [GPa/m^3], 2. $K_n = 10^4$ [GPa/m^3], 3. $K_n = 10^2$ [GPa/m^3]

We now turn our attention to Figs. 10.1 and 10.2. When the enhanced degrees of freedom are constrained (resulting in zero displacement jump) Eq. (26) then predicts zero stresses, compare Figs. 9.1 and 10.1. In the present example this is an artificial boundary condition and bears no relevance to the actual deformation of the beam. On the other hand, when running a crack propagation analysis, such a condition is generally applied at the crack tip to close the crack. This implies that conditions driving the crack analysis, such as maximum tensile stress, cannot be checked directly at the crack tip but in elements directly in front of the crack. The finite element mesh used in all above examples together with the deformation pattern for individual interfacial stiffnesses is displayed in Fig. 12.

The last set of results is again derived for the three-point bending test. Note that unlike the normal stresses for which the closed discontinuity is an undesirable condition (normal stress equal to zero on the beam surface) it provides correct results for shear stresses (zero shear on the beam surface). Moreover, Fig. 13 clearly shows the ability of the enhanced element to represent correctly, at least qualitatively, the singularity

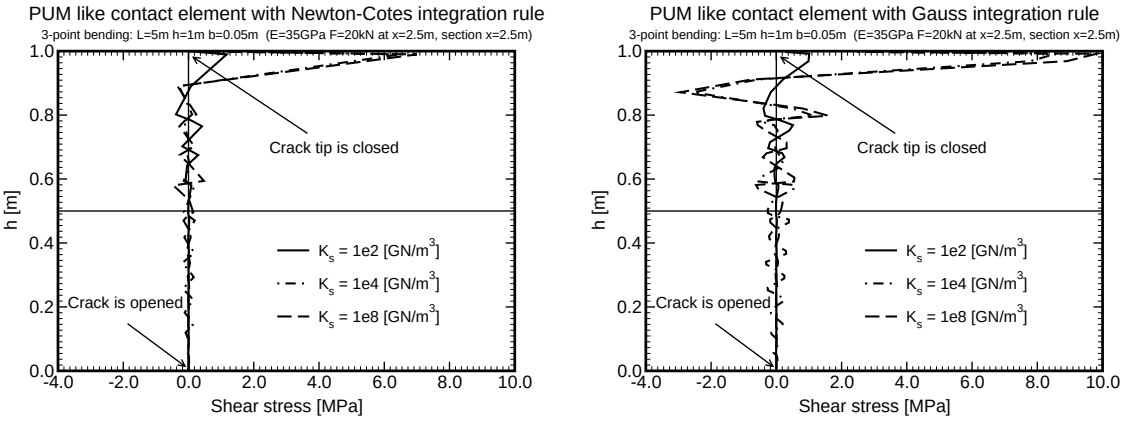

Fig. 13. 3-point bending - Distribution of shear stress in section B-B, Fig. 4

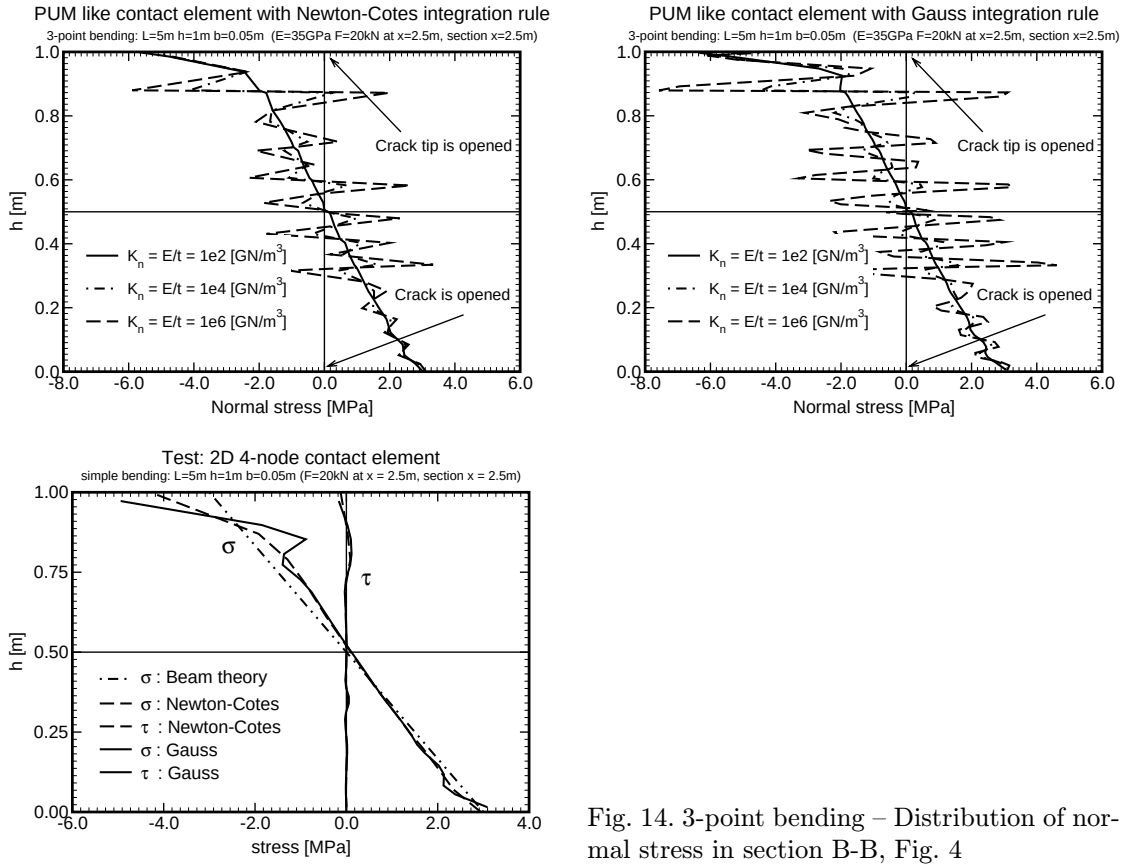

Fig. 14. 3-point bending – Distribution of normal stress in section B-B, Fig. 4

of the shear stress under the concentrated load. Note that there was a minor offset of the point of application of force and the discontinuity end point. Normal stresses

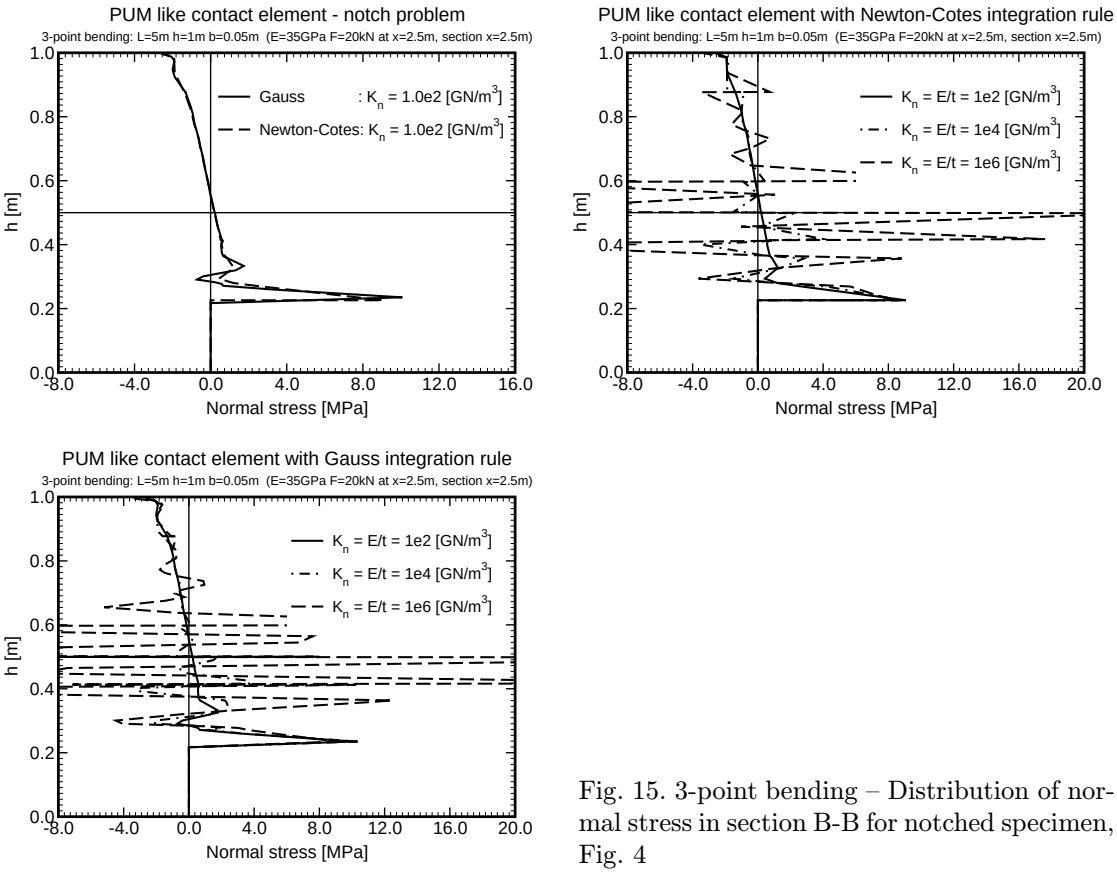

Fig. 15. 3-point bending – Distribution of normal stress in section B-B for notched specimen, Fig. 4

are plotted in Fig. 14 together with corresponding results derived with the interface element. Similar characteristics of the stress distribution as found for the four-point bending are recovered. Note that the results displayed in Figs. 14.1 and 14.2 were derived assuming the nonzero jump condition on both ends of the discontinuity. The results for the last example, the notch problem, are plotted in Fig. 15. When disregarding the typical oscillatory response of the enhanced triangular element with the high interfacial stiffness we arrive at the similar distributions of normal stresses in front of the notch as found with the conventional interface element, recall Fig. 8.

5 Algorithm of crack front tracking

This section briefly outlines the algorithmic aspects and data management for tracking the two-dimensional crack propagation. We assume that the geometry of the problem is described by a set of nodes, faces and elements and that each face is defined by its nodes and for each element we are provided with its nodes and faces. Having these data at our disposal, it appears to be most advantageous to store the crack path with respect to its position on selected faces. The resulting algorithm is then reasonably simple and easy to implement.

The following notation is extensively used in this section. We denote the set of all nodes in the problem as $\mathcal{N}$, the set of all faces as $\mathcal{F}$ and the set of all elements as $\mathcal{E}$ while n stands for individual nodes, f for faces and e for elements, respectively. Symbol $\mathcal{E}(f)$ is used for the set of all elements sharing a face f, $\mathcal{E}(n)$ is used for the set of all elements related to a node n, other sets will be denoted similarly. Further, $\mathcal{C}(n)$ denotes (possibly empty) set of all constraints (i.e., supports, prescribed displacements) related to a node n and $\mathcal{I}(e)$ the set of all element integration points. Symbols $\cup=$, $\setminus=$, $|=$ and $+=$ are used in C-language fashion to indicate a given operation with the result assigned to the left hand side.

5.1 Data initialization

For the sake of completeness, we include a brief description of data initiation for the given problem. Function **Init** extracts information necessary for the analysis of crack propagation from the set of elements $\mathcal{E}$, i.e., lists of elements related to a node (lines 2–3) and elements related to a face (lines 4–5). Finally, it creates the set $\mathcal{FC}$ which contains all faces crossed by a discontinuity.

```
   Init(E, f_0)
1  ForEach e ∈ E do
2      ForEach n ∈ N(e) do
3          E(n) ∪= {e}
4  ForEach f ∈ F(e) do
5      E(f) ∪= {e}
6  FC = {f_0}
```

5.2 Discontinuity insertion

The propagation of crack is driven by inserting strong discontinuities into elements which satisfy certain failure criteria. Therefore, **CrackElement** inserts a crack aligned at a given angle α to a given element e^c; f^c indicates the last face crossed by the discontinuity and ε is a certain positive parameter ensuring non-singularity of the element stiffness matrix (see Section 5). The function returns the element, in which the formation of discontinuity can occur in the next step (line 9).

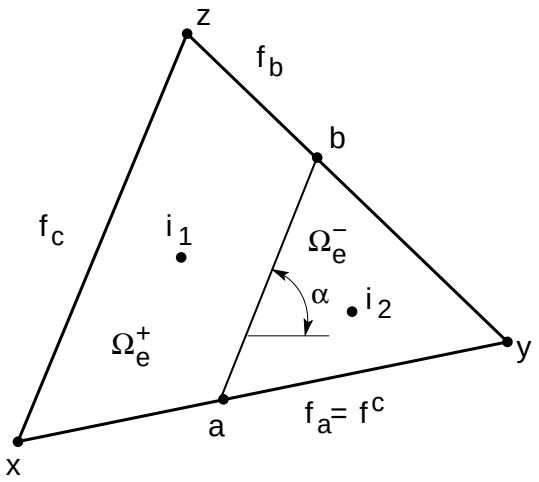

Fig. 16. Scheme of an enhanced element e_c

```
    CrackElement(e^c, f^c, α, ε, FC)
1   e^c.tag |= ENHANCED
2   fb = ComputeDiscontinuity(e^c, α, f^c)
3   MarkEnhancedNodes(f^c, fb, ε)
4   MarkNeighbouringElements(f^c, ε)
5   SetIntegrationPoints(e, f^c, fb)
6   RemoveDefaultConstraint(f^c)
7   AddDefaultConstraint(fb)
8   FC ∪= {fb}
9   return(E(fb)\{e^c})
```

In the first step (line 1), the element is tagged as `ENHANCED`* and the next face crossed by the discontinuity is determined (line 2). Then, nodes with enhanced degrees of freedom (line 3) together with neighboring elements (line 4) are determined. In the next step, location and weights of integration points are computed (line 5) and constraints resulting from prescribe zero values of enhanced degrees of freedom are updated (lines 6–7). Finally, the function for the determination of discontinuity position **ComputeDiscontinuity** is presented for the sake of clarity.

* Note that in the real code, this is accompanied by (re)allocation of various information related to the element.

```
   ComputeDiscontinuity(e, α, f^c)
1  a = GetCrackPos(f^c)
2  ForEach f ∈ {F(e)\f^c} do
3     IfGetIntersection(a, α, f) ≠ ∅
4        return(f)
```

5.3 Enhanced degrees of freedom management

Once a new face intersected by a crack (fb) is determined, the nodes on the previous crack face (fa) should be checked for the sign of the Heaviside function (lines 4–5) and for the possible enhancement by extended degrees of freedom (lines 6–7).

```
   MarkEnhancedNodes(fa, fb, ε)
1  a = GetCrackPos(fa)
2  b = GetCrackPos(fb)
3  ForEach n ∈ N(fa) do
4     If((ab⃗ × na⃗) · e⃗3) > 0
5        n.tag |= HEAVISIDE
6     IfCheckNodeSupport(n, ε) == TRUE
7        n.tag |= ENHANCED
```

The support of a basis function related to the nodes tagged as `ENHANCED` and `HEAVISIDE` in the previous procedure then contains elements which are not crossed by a discontinuity but are affected by the Heaviside function (see page 6), (lines 2–5). All nodes of such an element are enhanced by extra degrees of freedom (lines 6–8). Note that the degrees of freedom are not directly linked to the enhanced element and must be constrained to zero value (line 9).

```
   MarkNeighbouringElements(f)
1  ForEach n ∈ N(f) do
2     If(n.tag == ENHANCED) and (n.tag == HEAVISIDE)
3        ForEach e ∈ E(n) do
4           If e.tag ≠ ENHANCED
5              e.tag |= NEIGHBOR
6           ForEach ne ∈ N(e)
7              If ne.tag ≠ ENHANCED
8                 ne.tag |= ENHANCED
9                 C(ne) ∪= {DefaultConstraint}
```

The zero values of extended degrees of freedom are enforced by `DefaultConstraint`, i.e., a constraint which does not affect regular degrees of freedom but fixes values of ex-

tended degrees of freedom. Functions **RemoveDefaultConstraint** and **AddDefaultConstraint** are used to prescribe zero crack opening on a new crack face (**CrackElement**, line 7) and to constrain an element basis function for neighboring elements.

```
   RemoveDefaultConstraint(f)
1  ForEach n ∈ 𝒩(f) do
2     𝒞(n) \= {DefaultConstraint}

   AddDefaultConstraint(f)
1  ForEach n ∈ 𝒩(f) do
2     𝒞(n) ∪= {DefaultConstraint}
```

5.4 Integration points

In the original work (Wells and Sluys et al. 2001), a relatively complicated 23-point integration scheme was used for the numerical evaluation of individual integrals appearing in Eqs. (40)–(42). Our approach, however, is substantially simpler as it exploits the linearity of element basis functions (see Eq. (44)). Thus, the individual terms of element stiffness matrix remain constant on parts of element Ω_e^+ and Ω_e^- (the Heaviside function equal to 1/0) and the corresponding integration weights can be simply obtained as areas of Ω_e^+ and Ω_e^- (lines 8–9). The position of integration points is set to the center of quadrilateral $xabz$ (line 6) and triangle ayb (line 7), respectively. Finally, the sign of the Heaviside function for given integration points is determined in lines 11–12 of function **SetIntegrationPoints**.

```
   SetIntegrationPoints(e, fa, fb)
1  a = GetCrackPos(fa)
2  b = GetCrackPos(fb)
3  fc = ℱ(e)\ {fa ∪ fb}
4  {x, z} = 𝒩(fc)
5  y = 𝒩(e)\{x ∪ z}
6  i⃗1 = (a⃗ + b⃗ + x⃗ + z⃗)/4
7  i⃗2 = (a⃗ + b⃗ + y⃗)/3
8  i2.weight = GetTriangleArea(a, b, y)
9  i1.weight = GetTriangleArea(x, y, z) − i1.weight
10 ForEach i ∈ ℐ(e) do
11    If((i⃗a × a⃗b) · e⃗3) > 0
12       i.tag |= HEAVISIDE
```

5.5 Regularity of stiffness matrix

Based on numerical experiments reported in (Wells and Sluys et al. 2001), the support of a nodal basis function must fulfill certain conditions to ensure the non-singularity of element stiffness matrix. Specifically, both areas of support of the nodal basis function with the Heaviside function equal to 1 ($area^+$) or equal to 0 ($area^-$) must be large enough to prevent ill-conditioning of the stiffness matrix (line 12–15 of function **CheckNodeSupport** given below). In (Wells and Sluys et al. 2001), the value of $\varepsilon \approx 10^{-4}$ is suggested.

```
    CheckNodeSupport(n, ε)
1   ForEach e ∈ E(n) do
2       If e.tag == ENHANCED
3           ForEeach i ∈ I(e) do
4               If i.tag == HEAVISIDE
5                   area⁺ += i.weight
6               Else
7                   area⁻ += i.weight
8       ElseIf n.tag == HEAVISIDE
9           area⁺ += GetElementArea(e)
10      Else
11          area⁻ += GetElementArea(e)
12  If min(area⁺, area⁻) < ε(area⁺ + area⁻)
13      return(FALSE)
14  Else
15      return(TRUE)
```

6 Conclusion

The derivation of a simple constant strain triangle with embedded discontinuity was presented. Number of examples were analyzed to test the behavior of the element. In particular, the three-point and four-point bending tests were selected in the present study. The element was tested in view of its ability to replace a conventional interface element and thus avoid the need for structured meshes. To that end, normal and shear stresses developed along a predefined discontinuity, recall Figs. 4 and 5, were plotted. The final distributions were compared with the similar results provided by the interface element. Unlike the interface element, the present triangular element suffers from significant oscillations of discontinuity tractions, particularly when the the initially elastic behavior with zero discontinuity jumps is represented. This unwanted behavior is attributed to initially high interface stiffness (correct representation of elastic "undamaged" response corresponds to infinite interface stiffness). This undesirable effect is not satisfactorily solved when using the Newton-Cotes integration scheme in place of the more standard

Gauss integration scheme. On the other hand, when allowing for a certain "small" displacement jump along the discontinuity by reducing the interface stiffness the correct representation of interfacial tractions, normal and shear stresses in the present example problems, is recovered. This property is appealing and it might be expected that the enhanced element will perform well in applications where reduction of stiffness due to damage (cracks, shear bends) is expected. This will be the subject of the future work.

Acknowledgements. We would like to express our thanks to K. deProft and A. Simone for numerous interesting discussions and suggestions. Financial support for this project was provided by the GAČR 106/02/0678 grant.

REFERENCES

[1] BABUŠKA, I., BANERJEE, U., and OSBORN, J. E. (2001), "On Principles for the Selection of Shape Functions for the Generalized Finite Element Method." Report No. 01-16 TICAM.

[2] BABUŠKA, I. and MELENK, J. M. (1997), "The Partition of Unity Method." International Journal for Numerical Methods in Engineering *40,* 727–758.

[3] BITTNAR, Z. and ŠEJNOHA, J. (1996), "Numerical methods in structural engineering." ASCE Press.

[4] DE BORST, R. and MUHLHAUS, H. B. (1992), "Gradient dependent plasticity – formulation and algorithmic aspects." International Journal for Numerical Methods in Engineering *35,* 521–539.

[5] DE PROFT, K., DE WILDE, W. P., Sluys, L. J. (2002), "A combined damage-plasticity model for discontinuous modeling of fracture." Proceedings of the Fifth World Congress on Computational Mechanics (WCCM V), Mang, H. A., Rammerstorfer, F. G. and Eberhardsteiner, J., eds. Vienna University of Technology.

[6] DUARTE, C. A. and ODEN, J. T. (1996), "H-p clouds and h-p meshless method." Numerical Methods for Partial Differential Equations *12,* 521–539.

[7] MELENK, J. M. and BABUŠKA, I. (1996), "The Partition of Unity Finite Element Method: Basic Theory and Applications." Computer Methods in Applied Mechanics and Engineering *139,* 298–314.

[8] MOES, N., DOLBOW, J. and BELYTSCHKO, T. (1999), "A finite element method for crack growth without remeshing." International Journal for Numerical Methods in Engineering *46,* 131–151.

[9] OLIVER, J., CERVERA, M., MANZOLI, O. (1999), "Strong discontinuities and continuum plasticity models: The strong discontinuity approach." International Journal of Plasticity *15,* 131–151.

[10] OLIVER, J., HUESPE, A. E., PULIDO, M. D. G, and CHAVES, E. (2002), "From continuum mechanics to fracture mechanics: the strong discontinuity approach." Engineering Fracture Mechanics *69,* 131–151.

[11] PIJAUDIER-CABOT, G. and BAŽANT, Z. P. (1987), "Non local damage theory." ASCE Journal of Engineering Mechanics *113,* 1512–1533.

[12] SIMONE, A., REMMERS, J. J. C. and WELLS, G. N. (2001), "An interface element based on the partition of unity." Report No. CM2001.007, TU Delft.

[13] WELLS, G. N. and SLUYS, L. J. (2001), "A new method for modelling cohesive cracks." International Journal for Numerical Methods in Engineering *50,* 2667–2682.